

Tunneling-related electron spin relaxation in quantum-dot molecules

Michał Gawelczyk* and Krzysztof Gawarecki

*Department of Theoretical Physics, Faculty of Fundamental Problems of Technology,
Wrocław University of Science and Technology, 50-370 Wrocław, Poland*

We study theoretically the process of spin relaxation during phonon-assisted tunneling of a single electron in self-assembled InAs/GaAs quantum-dot molecules formed by vertically stacked dots. We find that the spin-flip tunneling rate may be as high as 1% of the spin-conserving one. By studying the dependence of spin relaxation rate on external fields, we show that the process is active at a considerable rate even without the magnetic field and scales with the latter differently than the relaxation in a Zeeman doublet. Utilizing a multiband $\mathbf{k}\cdot\mathbf{p}$ theory, we selectively investigate the impact of various spin-mixing terms in the kinetic carrier-phonon interaction Hamiltonians. As a result, we identify the main contribution to come from the Dresselhaus spin-orbit interaction, which is responsible for the zero-field effect. At magnetic fields above 10 T, this is surpassed by another contributions due to the structural shear strain. We study also the impact of the sample morphology and determine that the misalignment of the dots may enhance relaxation rate by over an order of magnitude. Finally, via virtual tunneling, the process in question affects also stationary electrons in tunnel-coupled structures and provides a Zeeman-doublet spin relaxation channel even without magnetic field.

I. INTRODUCTION

The dynamics of spin degrees of freedom in semiconductor nanostructures, mainly quantum dots (QDs), is motivated by both still not fully explored and understood physics of spin relaxation and decoherence as well as the potential role of such structures in spintronics and quantum information processing^{1,2}. Provided spin lifetimes of confined carriers are shown to be extraordinarily long, a promising application in spin-based memories additionally drives the interest³. While various types of QDs can be utilized for these purposes, self-assembled structures come with the possibility of optical control as they are optically active, as opposed to the, e.g., gated defined structures. This allows one to perform essential operation of initialization, manipulation and readout by means of light⁴⁻⁹, which provides very fast operation. Recently, much attention is focused on tunnel-coupled structures like QD molecules^{10,11}, as the coupling may be exploited in promising protocols developed for quantum-information processing^{12,13}.

While there is a considerable amount of theoretical works concerning spin relaxation of both types of carriers in single QDs of various types¹⁴⁻²⁰, the field of coupled QDs is far less explored in this context. Single existing studies concern the impact of the presence of the second QD with the resultant tunnel coupling and other effects on the spin relaxation in one of the QDs for the electron²¹ and hole²². Regarding phonon-assisted tunneling in quantum-dot molecules, although the physics of the orbital transition itself has been widely recognized²³⁻²⁸, studies concerning the behavior of spin states during tunneling are scarce. Those focus mostly on phonon induced spin pure dephasing during tunneling^{29,30} with a single

work containing a perturbative estimation of the rate of spin-orbit-induced spin-flip tunneling³¹.

Here, we focus on the phonon-assisted tunneling of electrons between coupled quantum dots and calculate the rate of such a transition affected by a simultaneous spin flip as compared to the spin-conserving one. Employing a multi-band theoretical $\mathbf{k}\cdot\mathbf{p}$ framework, we calculate electron states as well as their coupling to the acoustic-phonon bath and the resultant rates of dissipative transitions. Studying the dependence of the spin-flip tunneling rate on external fields, we find that it may be as high as 1% of the spin-conservative tunneling rate and its scaling with the magnetic field differs from that known from the Zeeman-doublet spin relaxation. Importantly, the effect takes place without the magnetic field at a considerable rate. By selectively enabling the spin-mixing terms in both kinetic-energy and carrier-phonon interaction Hamiltonians, we quantify the impact of various mechanisms of spin relaxation. Those, via the effective conduction band description, can be associated with perturbative and phenomenological interaction terms known from the literature. We find that up to $B \sim 15$ T the main contribution to spin relaxation comes from the opposite-spin admixtures to the electron ground state caused by the Dresselhaus spin-orbit interaction. At higher field, another source of admixtures becomes dominant, and that is the structural shear strain. Furthermore, we check the impact of typical details of morphology of self-assembled structures on spin relaxation, and find that the misalignment of dots may elevate the zero-field relaxation rate by an order of magnitude.

Finally, we also find that at nonzero temperatures the process in question strongly enhances spin relaxation in Zeeman doublets in each of the QDs via virtual repetitive tunneling affected by spin flips. In fact, we deal not only with a mere enhancement, but with a channel of spin relaxation without the magnetic field that may set the limit for spin lifetime of stationary carriers confined in tunnel-

*Electronic address: michal.gawelczyk@pwr.edu.pl

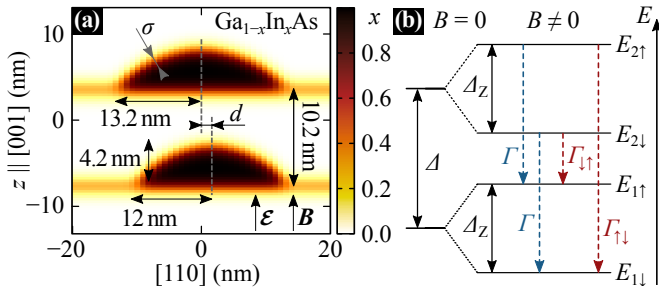


FIG. 1: (a) A cross-section of the material composition (color gradient) of the double QD structure in the $(1\bar{1}0)$ plane. (b) A schematic energy diagram of the system with relevant transitions marked with arrows.

coupled structures utilized currently in spintronics and quantum information protocols^{12,13}.

The paper is organized as follows. We begin in Sec. II with specifying the system, describing the theoretical model and providing general expectations regarding the results. Next, in Sec. III, we present and analyze the calculated spin relaxation rates, and their dependence on external fields as well as structural details of the quantum-dot molecule. Then, in Sec. IV, we show the crucial impact of studied transition on spin lifetime for stationary electrons in QDs forming the molecule. Finally, we conclude the paper in Sec. V.

II. SYSTEM AND MODEL

In this section, we characterize the system under study, and then describe the theoretical framework of our calculations as well as construct some general predictions regarding the results.

A. System

We model a self-assembled system of two vertically stacked flat-bottom dome-shaped InAs QDs embedded in a GaAs matrix, separated by the distance D . We assume a uniform composition of 100% InAs inside the QD and the 0.9 nm-thick wetting layer. The dots are of equal 4.2 nm height, while the upper QD is slightly wider with the base radius of 13.2 nm as compared to the bottom QD with $r = 12$ nm. We optionally account for planar misalignment of QDs by distance d and material diffusion at interfaces simulated by Gaussian averaging of the composition profile with the standard deviation σ . These features represent typical morphological details met in layered self-assembled QDs³². A cross-section of the resulting material composition is presented in Fig. 1(a), where QDs' dimension are also given. Unless otherwise stated, we will refer to the basic model of sharp-interface coaxial QDs with $d=0$ and $\sigma=0$. The structure is placed in axial electric $\mathcal{E} = \mathcal{E}\hat{z}$ and magnetic $\mathbf{B} = B\hat{z}$ fields.

B. Theoretical model

We follow a calculation scheme from structural modeling, through computation of the electron eigenstates, to evaluating the transition rates resulting from interactions with phonons. The strain distribution related to InAs/GaAs lattice mismatch is calculated within the standard continuous elasticity approach³³. Due to the lack of inversion symmetry in the zinc-blende crystal structure, the shear strain leads to appearance of the piezoelectric potential. We account for the latter in a nonlinear regime by including the strain-induced polarization field up to the second order terms in strain tensor elements³⁴, where the material parameters are taken from Ref. [35]. Having this included, we calculate the electron states using the eight-band envelope-function $\mathbf{k}\cdot\mathbf{p}$ theory^{36,37}. While the inclusion of electric field is straightforward, we incorporate a magnetic field to the Hamiltonian by standard Zeeman terms and by the Peierls substitution in the gauge-invariant scheme³⁸. Via numerical diagonalization, we obtain eigenvectors $\Psi(\mathbf{r})$ in the form of pseudospinors, components of which are the envelope functions within each of the respective subbands. Those may be classified with the Γ_{6c} , Γ_{8v} , and Γ_{7v} irreducible representations of T_d point group³⁹. The Γ_{6c} block in the Hamiltonian is related to the lowest conduction band, Γ_{8v} to the heavy- and light-hole, and Γ_{7v} to the spin-orbit split-off subbands. The Dresselhaus spin-orbit interaction is accounted for via perturbative terms added to H_{6c8v} and H_{6c7v} Hamiltonian blocks responsible for coupling of conduction band to valence bands³⁹. Finally, we include the impact of strain using the Bir-Pikus Hamiltonian with the standard a_c , a_v , b_v , and d_v deformation potentials^{40,41}. The explicit form of the Hamiltonian, material parameters and details of the numerical implementation of the model are given in the Appendix of Ref. [42].

To investigate spin relaxation due to phonon-assisted dissipative transitions, we take into account the interaction of electrons with the acoustic-phonon bath in the long-wavelength limit via the deformation-potential (DP) and piezoelectric (PE) couplings⁴³, both having the form of corrections to the Hamiltonian due to the phonon-induced strain field. The latter is plugged into the Bir-Pikus Hamiltonian to account for the DP coupling^{44,45}, while the PE interaction takes effect via the shear-strain-induced polarization field. The explicit form of the interaction Hamiltonian and detailed description of the formalism used may be found in Ref. [46]. The rates of transitions are found using the Fermi golden rule.

C. Initial qualitative considerations

The carrier-phonon interaction is spin-conserving and hence there is no direct phonon-induced coupling of electron states with opposite spins. However, such spin-off-diagonal terms appear in the effective conduction

band description after including coupling to the valence bands via the H_{6c8v} and H_{6c7v} blocks as well as spin-mixing terms in the valence-band block H_{8c8v} . Treating the latter within the quasi-degenerate perturbation theory⁴⁷, one finds higher-order terms that induce electron spin relaxation⁴⁸. While they are caused by various effects, these spin-flip channels can generally be divided into two classes of: *admixture* and direct *spin-phonon* mechanisms^{14,49}. Such distinction may be understood based on the separation into spin-conserving and perturbative spin-mixing parts, which is performed in both effective conduction-band Hamiltonians: the kinetic energy, $H_0 + H_1$, and the carrier-phonon interaction, $V_0 + V_1$. Then, up to the first order in perturbation, the overall effect is generated by pairs $H_1 + V_0$ and $H_0 + V_1$. The former is responsible for the admixture mechanisms: the perturbation in the kinetic term prevents spin from being a good quantum number as each of electron eigenstates achieves an admixture from the opposite-spin subband. Such states can then be coupled by spin-preserving interaction with phonons. The other combination describes the spin-phonon class of mechanisms, in which unperturbed electron states are coupled via the off-diagonal corrections to the interaction Hamiltonian (inherited after the Bir-Pikus H_{6c8v} and H_{6c7v} blocks). This may be in fact also thought of as dynamical induction of opposite-spin admixtures caused by phonons.

Calculation of spin relaxation rates within the Zeeman doublet in a single QD may be found in Ref. [50] along with decomposition into various sub-mechanisms and evaluation of their contributions. There, the admixture caused by the structural shear strain proved to be dominant source of spin flips. Here, we deal with another transition involving spin relaxation, and our aim is to similarly assess which channels are responsible for the effect. Understanding the sources of the two general spin relaxation channels allows us to have certain expectations. In the case of Zeeman doublet, one typically deals with the generic B^5 magnetic-field dependence of relaxation rate. This is followed by all sub-mechanisms if PE coupling to phonons is considered. The only contributions exhibiting another, B^7 scaling are those related to DP coupling within the admixture mechanism⁵⁰. The difference of 2 in the powers of B may be traced back to the dependence of phonon-spectral densities on transition energy: E and E^3 , respectively for PE and DP couplings, combined with the fact that for the doublet the whole energy difference is the Zeeman splitting proportional to B . The remaining power of 4 is related to the field-induced breaking of time-reversal symmetry. Let us consider a perturbation that generates the opposite-spin admixture to the electron eigenstate. In the presence of time-reversal symmetry the two states have to be reflections of one another, so the admixtures are of exactly equal magnitude and opposite phases. This cancels under the matrix element of the interaction Hamiltonian and hence does not lead to a transition. However, in the presence of magnetic field the symmetry is broken, what

yields a difference in admixture magnitudes in the two states with the leading contribution proportional to B^2 , which is reflected in the relaxation rate.

Here, we deal with tunneling with a finite transition energy, to which the Zeeman splitting forms only a minor contribution. Moreover, as the phonon spectral density for tunneling (or simply the tunneling rate), treated as a function of transition energy, is modulated by an oscillation with frequency related to the interdot distance ($\propto 1/D$, see the inset in Fig. 2), it is highly ambiguous how such a change in the transition energy affects the rate. Since the energy separation is on a single meV scale, we may also expect a more pronounced role of the DP coupling, while the PE contribution should be of lesser importance, contrarily to the Zeeman-doublet case. Moreover, the two states connected by the transition are located in different dots, hence there is no need to break the time-reversal symmetry for the admixture mechanism to take place. Thus, one may expect non-zero relaxation rate without magnetic field and a dependence on B different from the one observed for the case of the Zeeman doublet. This will be assessed with the help of calculated B -field dependence of relaxation rates.

III. SPIN RELAXATION DURING TUNNELING

In this section, we focus on the calculated rates of tunneling with spin relaxation by analyzing their dependence on external fields as well as determining the underlying mechanisms and their relative contributions to the overall effect.

A. Spin-flip tunneling rates

Having our initial predictions in mind, let us focus on the calculated rates of spin-flip tunneling. It is reasonable to consider as a figure of merit with practical meaning the relative rate, i.e., the ratio of rates for tunneling with ($\Gamma_{\uparrow\downarrow}$ or $\Gamma_{\downarrow\uparrow}$) and without (Γ) a spin flip

$$\tilde{\Gamma}_{\uparrow\downarrow/\downarrow\uparrow} = \frac{\Gamma_{\uparrow\downarrow/\downarrow\uparrow}}{\Gamma},$$

rather than the bare rate of the former, as these two processes always compete with each other. One deals in practice with partial loss of spin polarization that is well quantified by this measure. Here, the subscript refers to the two opposite spin-flip processes [see Fig. 1(b)]. To begin, we present in Fig. 2 the dependence of the two relative spin relaxation rates on the axial electric field at various magnitudes of the magnetic field. The first thing to notice is that, while nearly identical at $B = 1$ T, the two rates evolve differently with increasing magnetic field. In both cases, the uneven and shifted oscillations originate from the interplay of these in Γ (plotted in the inset), which are virtually independent of B , with those

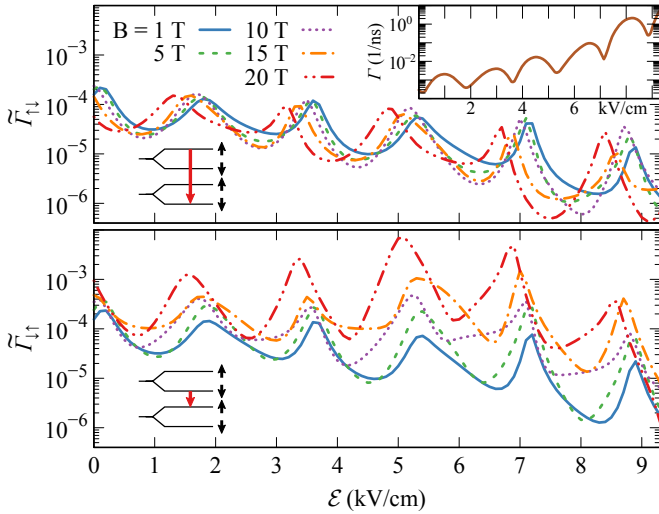


FIG. 2: The ratio of the spin-flip-accompanied to spin-preserving electron tunneling rates, $\tilde{\Gamma}_{\uparrow\downarrow}$ (top panel) and $\tilde{\Gamma}_{\downarrow\uparrow}$ (bottom), as a function of the axial electric field \mathcal{E} at various magnitudes of the magnetic field B . Inset: Spin-preserving tunneling rate F vs. the axial electric field. Results obtained for the sharp-interface double quantum dot at $T = 0$ K.

in $\Gamma_{\uparrow\downarrow/\downarrow\uparrow}$. The latter are shifted as the transition wanders along the spectral density with rising Zeeman splitting. Apart from this interplay, the transition $\uparrow\downarrow$ shifts to higher energies, where coupling to acoustic phonons is weaker, while the opposite occurs for the other, $\downarrow\uparrow$ transition. This underlies the seemingly counter-intuitive fact that the relaxation of the electron spin towards the magnetic field is more efficient than the opposite „natural“ process. Moreover, based on the above reasoning, transition-energy shifts alone should lead to enhancement of one of the rates and reduction of the other. Instead, we deal with approximately unchanged values of the latter, which affected only by horizontal shifts in the electric-field domain. Thus, it is reasonable to presume a global dependence on B of a nature that is not related to the specific character of the phonon spectral density for tunnel transitions. This, however, requires a more detailed analysis. Just before we switch to it, let us emphasize that $\tilde{\Gamma}_{\downarrow\uparrow}$ can reach values as high as 10^{-2} .

B. Magnetic-field dependence

To systematically examine the magnetic-field dependence of spin relaxation rates, we need a more synthetic figure of merit, which would be immune to variations due to moving along the oscillating spectral density with rising Zeeman splitting. The latter has an evident impact on $\tilde{\Gamma}_{\uparrow\downarrow/\downarrow\uparrow}$ and is unavoidable in practice, but its origin is unrelated to any channels of spin relaxation. Therefore, in Fig. 3, we plot the ratio in which both of the rates, $\Gamma_{\uparrow\downarrow}$ and F are calculated for the same transition energy. This

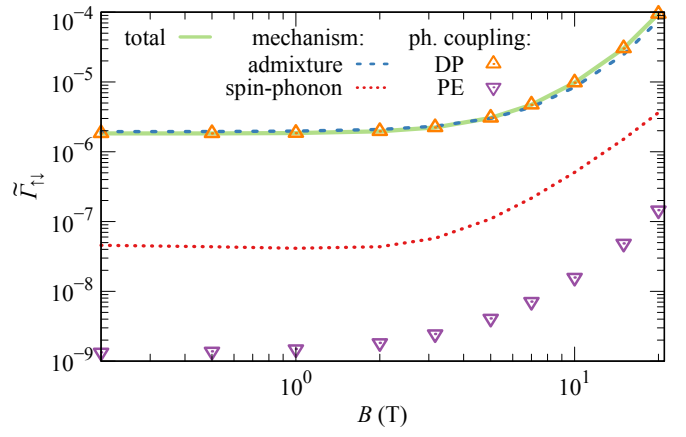


FIG. 3: The total relative spin-flip tunneling rate $\tilde{\Gamma}_{\uparrow\downarrow}$ (solid line) compared to those arising from the admixture (dashed) and spin-phonon (dotted) mechanisms only as well as divided into contributions due to the deformation-potential (\triangle) and piezoelectric (∇) couplings to phonons, plotted as a function of the magnetic field; calculated for the sharp-interface double quantum dot at $T = 0$ K.

is achieved by tuning the electric field to compensate for the Zeeman splitting. The choice of $E=4.812$ meV results from the fact that it corresponds to the last (closest to the tunneling resonance) maximum in F that is available for spin-flip tunneling at fields up to $B=20$ T, as the resonance in this case becomes wider with B . Apart from the total rate (solid line), we also plot those arising from the admixture (dashed) and spin-phonon (dotted) channels treated separately. As predicted, there is a nonzero rate of spin relaxation at $B \rightarrow 0$ T. Although it is not shown here, so as not to dim the picture, the value has been checked down to $B = 10^{-4}$ T and remains constant up to numerical precision. We find the total rate as dominated by the admixture channel, similarly to the case of spin relaxation in the Zeeman doublet⁵⁰, with approximately 1.5 order of magnitude smaller spin-phonon contribution. It should be noted here that rates due to various mechanisms are not strictly additive, as interactions may add up also destructively as well as the total effect may overcome sum of individual contributions if those enter via nonlinear terms in the Hamiltonian. However, such a significant difference in magnitudes allows us to determine the dominant channel without doubt. Additionally, we split the total rate into the contributions due to DP and PE couplings (symbols). These are additive, and we deal with almost negligible PE contribution to the rate generated by the DP coupling, which is understandable considering the transition energy exceeding the range of efficient PE interaction. The latter is subject to change for systems with narrower tunneling resonance, e.g., with larger interdot distance or bigger difference between the two dots. However, as this comes with strongly reduced tunneling rates, such structures are of lesser interest. Regarding the dependence on the magnetic field at its higher

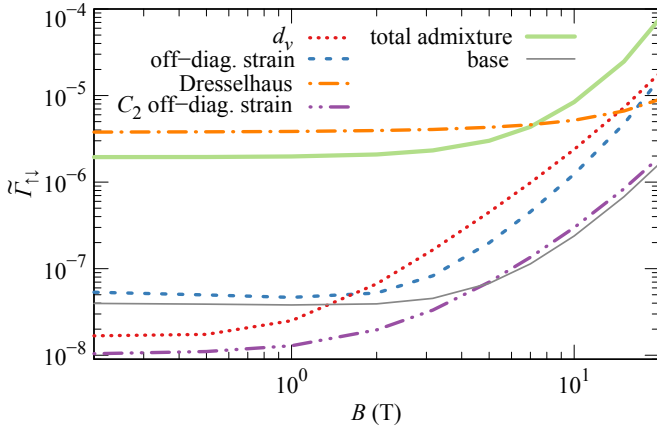


FIG. 4: The relative spin-flip tunneling rate due to the admixture mechanism (solid line) compared to the rates resulting from each of its constituent couplings in the valence band and band-off-diagonal blocks of the $\mathbf{k}\cdot\mathbf{p}$ Hamiltonian, plotted as a function of the magnetic field B ; calculated for the electron in the sharp-interface double quantum dot at $T = 0$ K.

magnitudes, it is difficult to assess it for the total (and admixture-induced) rate. While it tends to scale as B^4 above 10 T, it is impossible to reproduce the moderate-field-range behavior with an $aB^4 + c$ dependence. On the other hand, the spin-phonon-induced rate follows a well-defined $B^3 + c$ trend. Thus, the unclear behavior has to come from the admixture contribution.

C. Contributions to the relaxation rate

The opposite-spin admixtures, responsible here for most of the relaxation rate, may have multiple sources. For the case of relaxation within the Zeeman doublet, in large unstrained gate-defined QDs, the admixtures were found to originate mainly from the Dresselhaus spin-orbit interaction¹⁴. This is also the main reason for the spin-flip that accompanies electron $p \rightarrow s$ orbital relaxation in such kind of QDs⁴⁹. On the other hand, in smaller self-assembled dots like those considered here, almost entire rate was identified to originate from shear-strain-induced couplings between the conduction band and valence bands (via H_{6c8v} and H_{6c7v} Hamiltonian blocks) as well as among the valence bands through terms proportional to the d_v deformation potential in H_{8v8v} and H_{8v7v} . In the picture of effective description for conduction band, both these contributions turned out to have the form of a strain-induced correction to the electron Landé tensor, which is known from literature^{51,52}. To find sources of spin-mixing admixtures in the case of tunneling transition, we plot in Fig. 4 the magnetic-field dependence of relative relaxation rates due to the admixture mechanism. Apart from the total rate, we show also the contribution due to various couplings calculated by disabling all the respective matrix elements in

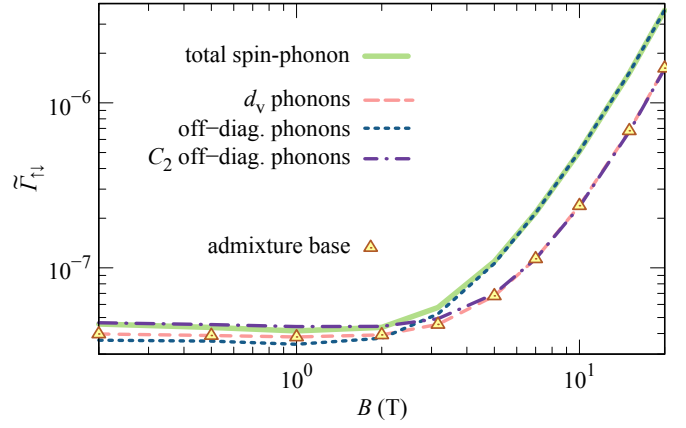


FIG. 5: The relative spin-flip tunneling rate due to the spin-phonon mechanism (solid line) compared to the rates resulting from each of its constituent couplings in the valence band, plotted as a function of the magnetic field B ; calculated for the electron in the sharp-interface double quantum dot at $T = 0$ K. Additionally, points show the base admixture contribution.

the Hamiltonian but the one in question. One may notice that all the rates are non-vanishing at $B \rightarrow 0$, with the pronounced domination of the Dresselhaus spin-orbit interaction in a wide range of fields up to $B = \sim 15$ T. Via fitting with $aB^m + c$, we find an exponent of $m = 2$ which, along with the order of magnitude of $\tilde{\Gamma}_{\uparrow\downarrow}$, is in agreement with the recent perturbative calculation concerning this channel³¹. At higher fields, the Dresselhaus contribution is surpassed by those arising from shear-strain-induced couplings between the conduction and valence bands and among the latter (dashed and dotted lines, respectively), which are those mechanisms that were found to dominate in the case of relaxation in the Zeeman doublet⁵⁰. As both have the effective form of corrections to the electron Landé tensor their stronger scaling with B is reasonable. We need to stress out here that there are some residual spin-mixing terms that cannot be explicitly turned off in our calculation. These, containing mainly the Rashba spin-orbit coupling due to structural asymmetry, alone give rise to the rate plotted with a thin gray line labeled as „base”. Since this, each of the rates obtained for the other mechanisms carries such an implicit contribution. While it is negligible for the Dresselhaus-induced dominant rate, it may be at least partially responsible for the values of others at $B \rightarrow 0$. This would be again in agreement with the interpretation of the shear-strain-induced contribution in terms of effective corrections to the g -factor, in view of which their impact should vanish at $B \rightarrow 0$.

The second class of spin-phonon mechanisms is responsible for the dominant Zeeman-doublet spin relaxation channel in large unstrained quantum dots⁴⁹. Here it plays a minor role, similarly to the case of doublet spin relaxation in single self-assembled dots⁵⁰. Nonetheless, let us analyze this contribution in detail with help of Fig. 5,

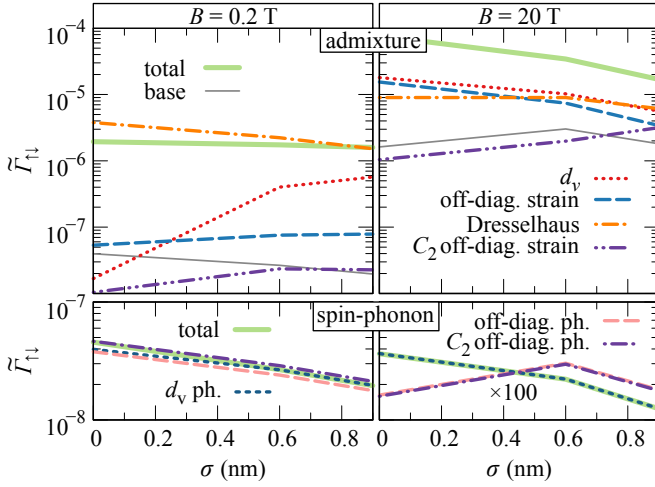


FIG. 6: The relative spin-flip tunneling rates due to individual mechanisms and their combinations at $B = 0.2$ T (left panels) and $B = 20$ T (right panels) and $T = 0$ K plotted as a function of the interfacial material intermixing length σ . The top (bottom) row of panels presents rates due to mechanisms from the admixture (spin-phonon) class.

where we plot the relative spin relaxation rates due to various spin-phonon mechanism. These split similarly to the strain-induced admixtures, as they enter via equivalent Hamiltonian matrix elements, but with a strain field coming from a different source: phonons instead of structural lattice deformation. From about $B = 0$ T the rate is dominated by the contribution, in which the phonon-induced shear strain enters via off-diagonal block element of the interaction Hamiltonian that couples conduction band to valence bands. Similarly, to the admixture case, this mechanism may be interpreted as a correction to the electron g -factor, which here is dynamically induced by the phonon strain field. Regarding the low-field regime, it is ambiguous whether we deal with nonzero contribution at $B \rightarrow 0$. Let us recall that there are some admixture sources (mainly Rashba spin-orbit coupling) that may not be switched off in our calculation. Those form the „base” contribution to the admixture-induced spin relaxation rate, which is unavoidably present also here and plotted with symbols for comparison. In view of this, it is reasonable to assume that at least most of the low-field spin-phonon rate is in fact due to the residual admixtures.

D. Impact of structure morphology

Having analyzed the overall results obtained for the ideal structure, we now focus on the impact of typical morphological features met in coupled QDs on spin relaxation during tunneling. The material interface of self-assembled QDs is never sharp due to the diffusion of atoms. We simulate this by Gaussian averaging of the material composition that leads to soft interface with the characteristic length of intermixing σ . To assess how

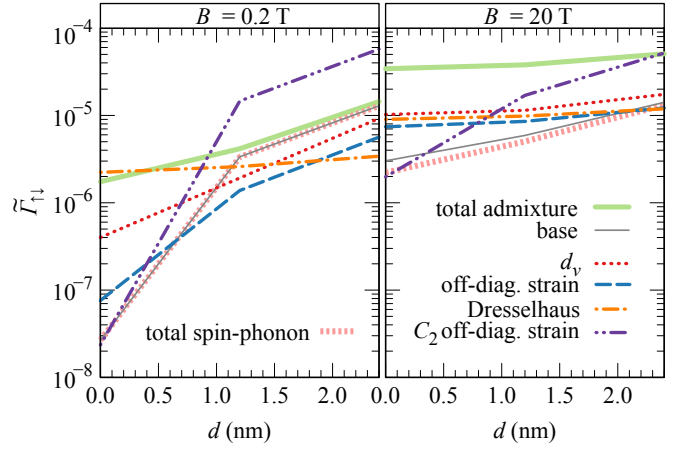


FIG. 7: The relative spin-flip tunneling rates due to individual mechanisms and their combinations at $B = 0.2$ T (left panel) and $B = 20$ T (right panel) and $T = 0$ K plotted as a function of the planar misalignment of the dots d .

it affects the individual spin-relaxation mechanisms, we plot in Fig. 6 the calculated relative rates versus σ for two values of the magnetic-field magnitude $B = 0.2$ T (left panels) and $B = 20$ T (right) representing the low- and high-field regimes. We begin with analyzing the admixture mechanism. Although one could expect that softer interfaces should lead to a reduction of shear strain, at low field we observe an increase of the rate related to the latter. While the expectation is basically correct, the most significant result of interface softening is the enhancement of penetration of the wave function into the barrier, where it experiences the impact of strain located on the interface. This is, however, compensated for by a decrease of the contribution due to the Dresselhaus spin-orbit interaction, and the total rate is approximately σ -independent. At the high field both shear-strain-induced rates are decreasing, which may be understood as the barrier penetration is prevented due in-plane shrinkage of wave functions in the magnetic field combined with reduced strain magnitude. In the case of rates induced by spin-phonon mechanisms, we deal with a very weak impact of the interface softening.

Another feature of self-assembled quantum dot molecules is the misalignment of the dots. In Fig. 7, we analyze the impact of the latter, quantified with the distance d on the relative spin relaxation rates. While the impact at the high field is minor, we deal with a significant increase of all the admixture contributions in the low-field regime resulting from the symmetry lowering. Here, we do not split the spin-phonon induced effects into sub-mechanism as the difference between those rates is not noticeable in the scale of the overall variation of values. However, we plot the total spin-phonon-induced rate to notice, that at the low field it is in fact caused by the residual admixtures („base”), as mentioned above, as the two coincide perfectly.

E. Relaxation at nonzero temperature

Trivially, all rates of phonon-assisted transitions depend on temperature via the Bose distribution. This applies to both spin-preserving and spin-flip tunneling, thus the ratio of their rates undergoes a weak dependence induced by the mismatch of transition energies equal twice the Zeeman splitting,

$$\tilde{\Gamma}_{\uparrow\downarrow/\downarrow\uparrow}|_T = \tilde{\Gamma}_{\uparrow\downarrow/\downarrow\uparrow}|_{T=0\text{K}} \frac{|n_B(\Delta \pm \Delta_Z, T) + 1|}{|n_B(\Delta, T) + 1|},$$

where the sign distinguishes between opposite spin-flip processes. The factor on the right-hand side saturates with temperature, at low and moderate magnetic fields to a value close to 1. At $B = 20$ T the room-temperature values are around 0.67 and 2.3, respectively, for the given DQD with $g \approx 2.41$ and Δ set to 4.812 meV. Thus, with rising temperature the overbalance of the $\downarrow\uparrow$ relaxation is even enhanced.

IV. ENHANCEMENT OF ZEEMAN-DOUBLET SPIN RELAXATION

In this section, we show that the process of spin-flip tunneling investigated here affects electron spin not only during the transition, but has impact also on the stationary electron located in one of the QDs, which leads to additional channel of spin relaxation in the Zeeman doublet.

Let us consider an electron that does not actually tunnel, but stays approximately in its orbital ground state in the lower-energy QD. Exposed to the phonon-assisted tunnel coupling to the other dot, such an electron occupies at finite temperature a mixture of states localized in the two dots, which dominated by the ground state, according to the detailed balance condition. Provided the tunneling rates in both directions are finite, the electron continuously undergoes a virtual process of repetitive tunneling between the dots, which is affected by spin flips of the nature discussed in previous sections. This additional channel should enhance spin relaxation in the ground-state Zeeman doublet. To quantify the effect, we consider a set of rate equations for the four-level system, to which we insert the numerically calculated rates of all spin-preserving and spin-flipping transitions. Solving these via the Laplace transform method, we find an exponential component in the ground-state spin evolution, which describes the effective spin relaxation within Zeeman doublet. In Fig. 8, we plot the resulting spin relaxation rates $\gamma_{\uparrow\downarrow} = 1/T_1$ for three values of magnetic field: $B = 10^{-4}$ T, 0.1 T, and 1 T at application-relevant temperatures as a function of the axial electric field in the previously considered range close to the tunneling resonance. Starting from the highest magnetic-field case, we notice plateaus where the rate is weakly enhanced compared to the bare direct spin flip (plotted with the thin gray line for $T = 300$ K for comparison). At elevated

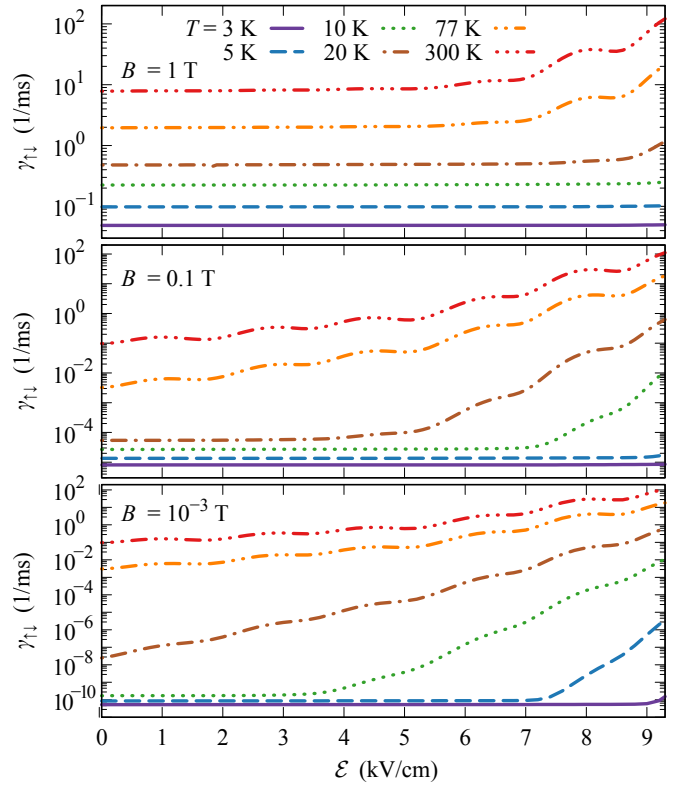


FIG. 8: The rate of spin relaxation in the orbital ground state Zeeman doublet, $\gamma_{\uparrow\downarrow} = 1/T_1$, in the lower-energy QD, plotted as a function of the axial electric field \mathcal{E} at various temperatures T for $B = 1$ T (top panel), $B = 0.1$ T (middle) and $B = 10^{-4}$ T (bottom).

temperatures, the rate increases as the system get pushed towards the tunneling with rising electric field. The lower the magnetic-field the more pronounced the role of the discussed spin relaxation channel is, which is simply due to the vanishing rate of the direct spin flip. Importantly, close to the resonance, the calculated rate very weakly depends on B and provides a spin relaxation channel at $B \rightarrow 0$ with rates reaching $\sim 10^{-2} \text{ ms}^{-1}$ at $T = 5$ K and over $\sim 10^2 \text{ ms}^{-1}$ at $T = 300$ K.

For a better insight, we set the electric field to $\mathcal{E} = 8.3 \text{ kV/cm}$, corresponding to the local maximum of the tunneling rate [see inset in Fig. 2], and in Fig. 9 we plot the effective spin relaxation rates as a function of magnetic field at various temperatures. Confronting the effective rates with those of direct spin flip plotted with gray lines for the two most outlying of simulated temperatures, we may notice how the virtual channel plays a dominant role in the low and moderate field range, on top of the standard B^5 direct spin-flip rate.

V. CONCLUSIONS

We have investigated theoretically the electron confined in a self-assembled double QD system and presented

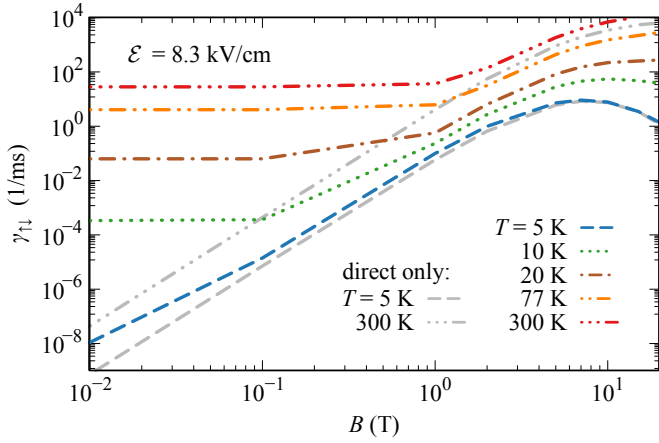


FIG. 9: The rate of spin relaxation in the ground-state Zeeman doublet, $\gamma_{\uparrow\downarrow}=1/T_1$, in the lower-energy QD, plotted as a function of the magnetic field B at various temperatures T for $\mathcal{E} = 8.3$ kV/cm. Light gray lines show the rate of bare direct phonon-induced spin relaxation for selected temperatures.

the calculated rates of tunneling transition with simultaneous spin flip as compared to the spin-preserving process. Using a multiband $\mathbf{k}\cdot\mathbf{p}$ theory and including the coupling to acoustic phonons with all leading-order spin-perturbing effects included, we have calculated the electron states, and the rates of transitions between them. By checking the dependence of the investigated spin-flip tunneling rate on external fields, we have determined that it can reach 1% of the spin-preserving one. Most importantly, it does not vanish even at $B \rightarrow 0$. Our theoret-

ical framework allowed us to selectively turn on various spin-mixing terms both in kinetic-energy and interaction Hamiltonians, so we could assess the relative contribution of individual spin relaxation mechanisms. Unlike the Zeeman-doublet case studied before, we have found that the Dresselhaus spin-orbit interaction is responsible for most of the spin relaxation in wide range of magnetic field magnitudes. At about $B = \sim 15$ T, it gets surpassed by the interactions induced by the structural shear strain, which, via the effective conduction-band description, may be understood as corrections to the electron g -factor. Considering the morphology of realistic self-assembled quantum-dot molecules, we have learned that planar misalignment of the dots strongly enhances the low-field spin relaxation rate by over an order of magnitude for a typical sample geometry. Finally, we have shown that at nonzero temperatures the studied process leads also to the Zeeman-doublet spin relaxation for stationary electrons via virtual tunneling to the other dot. This provides a phonon-related source of spin flips at zero magnetic field, which crucially depends on temperature.

Acknowledgments

We acknowledge support from the Polish National Science Centre under Grant No 2014/13/B/ST3/04603. Numerical calculations have been carried out using resources provided by Wroclaw Centre for Networking and Supercomputing (<http://wcss.pl>), Grant No. 203. We are grateful to Paweł Machnikowski for valuable discussions and advice.

- ¹ D. Loss and D. P. DiVincenzo, *Phys. Rev. A* **57**, 120 (1998).
- ² P. Recher, E. V. Sukhorukov, and D. Loss, *Phys. Rev. Lett.* **85**, 1962 (2000).
- ³ M. Kroutvar, Y. Ducommun, D. Heiss, M. Bichler, D. Schuh, G. Abstreiter, and J. J. Finley, *Nature* **432**, 81 (2004).
- ⁴ M. V. G. Dutt, J. Cheng, B. Li, X. Xu, X. Li, P. R. Berman, D. G. Steel, A. S. Bracker, D. Gammon, S. E. Economou, R.-B. Liu, and L. J. Sham, *Phys. Rev. Lett.* **94**, 227403 (2005).
- ⁵ A. Greilich, R. Oulton, E. A. Zhukov, I. A. Yugova, D. R. Yakovlev, M. Bayer, A. Shabaev, A. L. Efros, I. A. Merkulov, V. Stavarache, D. Reuter, and A. Wieck, *Phys. Rev. Lett.* **96**, 227401 (2006).
- ⁶ M. Atature, *Science* **312**, 551 (2006).
- ⁷ M. Kroner, K. M. Weiss, B. Biedermann, S. Seidl, S. Manus, A. W. Holleitner, A. Badolato, P. M. Petroff, B. D. Gerardot, R. J. Warburton, and K. Karrai, *Phys. Rev. Lett.* **100**, 156803 (2008).
- ⁸ X. Xu, B. Sun, P. R. Berman, D. G. Steel, A. S. Bracker, D. Gammon, and L. J. Sham, *Nat. Phys.* **4**, 692 (2008).
- ⁹ A. J. Ramsay, S. J. Boyle, R. S. Kolodka, J. B. B. Oliveira, J. Skiba-Szymanska, H. Y. Liu, M. Hopkinson, A. M. Fox,

- and M. S. Skolnick, *Phys. Rev. Lett.* **100**, 197401 (2008).
- ¹⁰ Q. Xie, A. Madhukar, P. Chen, and N. P. Kobayashi, *Phys. Rev. Lett.* **75**, 2542 (1995).
- ¹¹ H. J. Krenner, M. Sabathil, E. C. Clark, A. Kress, D. Schuh, M. Bichler, G. Abstreiter, and J. J. Finley, *Phys. Rev. Lett.* **94**, 057402 (2005).
- ¹² S. E. Economou, J. I. Climente, A. Badolato, A. S. Bracker, D. Gammon, and M. F. Doty, *Phys. Rev. B* **86**, 085319 (2012).
- ¹³ K. M. Weiss, J. M. Elzerman, Y. L. Delley, J. Miguel-Sanchez, and A. Imamoglu, *Phys. Rev. Lett.* **109**, 107401 (2012).
- ¹⁴ A. V. Khaetskii and Y. V. Nazarov, *Phys. Rev. B* **64**, 125316 (2001).
- ¹⁵ L. M. Woods, T. L. Reinecke, and Y. Lyanda-Geller, *Phys. Rev. B* **66**, 161318 (2002).
- ¹⁶ H. Westfahl, A. O. Caldeira, G. Medeiros-Ribeiro, and M. Cerro, *Phys. Rev. B* **70**, 195320 (2004).
- ¹⁷ J. L. Cheng, M. W. Wu, and C. Lü, *Phys. Rev. B* **69**, 115318 (2004).
- ¹⁸ E. Zipper, M. Kurpas, J. Sadowski, and M. M. Maška, *J. Phys. Condens. Matter* **23**, 115302 (2011).
- ¹⁹ H. Wei, M. Gong, G.-C. Guo, and L. He, *Phys. Rev. B* **85**, 045317 (2012).

- ²⁰ W.-P. Li, S.-J. Li, J.-W. Yin, Y.-F. Yu, and Z.-W. Wang, *Solid State Commun.* **192**, 1 (2014).
- ²¹ V. N. Stavrou, *J. Phys. Condens. Matter* **30**, 455301 (2018).
- ²² C. Segarra, J. I. Climente, F. Rajadell, and J. Planelles, *J. Phys. Condens. Matter* **27**, 415301 (2015).
- ²³ Z.-J. Wu, K.-D. Zhu, X.-Z. Yuan, Y.-W. Jiang, and H. Zheng, *Phys. Rev. B* **71**, 205323 (2005).
- ²⁴ V. López-Richard, S. S. Oliveira, and G.-Q. Hai, *Phys. Rev. B* **71**, 075329 (2005).
- ²⁵ V. N. Stavrou and X. Hu, *Phys. Rev. B* **72**, 075362 (2005).
- ²⁶ J. I. Climente, A. Bertoni, G. Goldoni, and E. Molinari, *Phys. Rev. B* **74**, 035313 (2006).
- ²⁷ A. Grodecka-Grad and J. Förstner, *Phys. Rev. B* **81**, 115305 (2010).
- ²⁸ K. Gawarecki, M. Pochwała, A. Grodecka-Grad, and P. Machnikowski, *Phys. Rev. B* **81**, 245312 (2010).
- ²⁹ M. Gawelczyk, M. Krzykowski, K. Gawarecki, and P. Machnikowski, *Phys. Rev. B* **98**, 075403 (2018).
- ³⁰ M. Gawelczyk, *Acta Phys. Pol. A* **134**, 926 (2018).
- ³¹ M. Gawelczyk and P. Machnikowski, *Semicond. Sci. Technol.* **32**, 045005 (2017).
- ³² H. J. Krenner, S. Stuffer, M. Sabathil, E. C. Clark, P. Ester, M. Bichler, G. Abstreiter, J. J. Finley, and A. Zrenner, *New J. Phys.* **7**, 184 (2005).
- ³³ C. Pryor, J. Kim, L. W. Wang, A. J. Williamson, and A. Zunger, *J. Appl. Phys.* **83**, 2548 (1998).
- ³⁴ G. Bester, X. Wu, D. Vanderbilt, and A. Zunger, *Phys. Rev. Lett.* **96**, 187602 (2006).
- ³⁵ M. A. Caro, S. Schulz, and E. P. O'Reilly, *Phys. Rev. B* **91**, 075203 (2015).
- ³⁶ M. G. Burt, *J. Phys. Condens. Matter* **4**, 6651 (1992).
- ³⁷ B. A. Foreman, *Phys. Rev. B* **48**, 4964 (1993).
- ³⁸ T. Andlauer, R. Morschl, and P. Vogl, *Phys. Rev. B* **78**, 075317 (2008).
- ³⁹ R. Winkler, *Spin-Orbit Coupling Effects in Two-Dimensional Electron and Hole Systems* (Springer, Berlin, Heidelberg, 2003).
- ⁴⁰ G. Bir and G. Pikus, *Symmetry and Strain-induced Effects in Semiconductors*, A Halsted Press book (Wiley, 1974).
- ⁴¹ T. B. Bahder, *Phys. Rev. B* **41**, 11992 (1990).
- ⁴² K. Gawarecki, *Phys. Rev. B* **97**, 235408 (2018).
- ⁴³ A. Grodecka-Grad, L. Jacak, P. Machnikowski, and K. Roszak, in *Quantum Dots: Research Developments*, edited by P. Ling (Nova Science Publishers, 2005) p. 47.
- ⁴⁴ L. M. Woods, T. L. Reinecke, and R. Kotlyar, *Phys. Rev. B* **69**, 125330 (2004).
- ⁴⁵ K. Roszak, V. M. Axt, T. Kuhn, and P. Machnikowski, *Phys. Rev. B* **76**, 195324 (2007).
- ⁴⁶ K. Gawarecki and M. Krzykowski, "Spin-orbit coupling and spin relaxation of hole states in [001]- and [111]-oriented quantum dots of various geometry," (2018), [arXiv:1809.09062](https://arxiv.org/abs/1809.09062).
- ⁴⁷ P.-O. Löwdin, *J. Chem. Phys.* **19**, 1396 (1951).
- ⁴⁸ A. Mielnik-Pyszczorski, K. Gawarecki, and P. Machnikowski, *Sci. Rep.* **8** (2018), [10.1038/s41598-018-21043-3](https://doi.org/10.1038/s41598-018-21043-3).
- ⁴⁹ A. V. Khaetskii and Y. V. Nazarov, *Phys. Rev. B* **61**, 12639 (2000).
- ⁵⁰ A. Mielnik-Pyszczorski, K. Gawarecki, M. Gawelczyk, and P. Machnikowski, *Phys. Rev. B* **97**, 245313 (2018).
- ⁵¹ J. H. Van Vleck, *Phys. Rev.* **57**, 426 (1940).
- ⁵² L. M. Roth, *Phys. Rev.* **118**, 1534 (1960).